



Neoproterozoic Granitoids of Bundelkhand Craton, India: Geochemistry and Geodynamic Settings

Sumit Mishra¹, Pradip K Singh^{2*}, Vinod K Singh³, Alexander I Slabunov⁴, HC Nainwal¹ and Neeraj Chaudhary³

¹Department of Geology, Hemvati Nandan Bahuguna Garhwal University, India

²División de Geociencias Aplicadas, Instituto Potosino de Investigación Científica y Tecnológica (IPICYT), Mexico

³Department of Geology, Institute of Earth Science, Bundelkhand University, India

⁴Institutes of Geology, Karelian Research Centre, Russia

*Corresponding author: Pradip K Singh, División de Geociencias Aplicadas, Instituto Potosino de Investigación Científica y Tecnológica (IPICYT), Camino a la Presa, San José 2055, San Luis Potosí, Mexico

Submission: July 02, 2017; Published: October 17, 2018

Abstract

The potash-rich granite and granodiorite-granite series rocks are extensively exposed in the Bundelkhand granite-greenstone belt around Jhansi, Babina and Mauranipur in the central part of the craton, which are mostly calc-alkaline in nature, relatively high Sr (12–436ppm), low Y (9.1–67) and low Sr/Y (0.24–21.37) ratio characteristics. These rocks have high Rb (77.7–539), moderate Nb (7.2–42.2) and Nd (21.92–115), and geochemically vary from mostly I- to A-type granites generally formed during syn- to post-collision. The chondrite normalized rare earth element distribution pattern is poorly fractionated $La_N/Lu_N = (3.4–31.79)$ with a negative Europium (Eu) anomaly ($Eu/Eu^* = 0.2–0.82$) showing subduction environment. The granodiorite-granite series rocks show mostly volcanic arc setting while potash-rich-granites plots within the syn-collision to post-collisional granite fields on the Yb+Ta versus Rb and Nb versus Y discrimination diagram. Geochemical characteristics indicate that anhydrous partial melting of the Paleoproterozoic Tonalite-trondhjemite-granodiorite or mafic crust through subduction setting responsible for formation of these rocks.

Keywords: Neoproterozoic granitoids; Subduction tectonics; Geodynamics settings; Bundelkhand Craton

Introduction

The early earth crust formation still remains immense wide scope for in depth research on the Precambrian crustal growth which evolved a wide range of geological processes including plate tectonics and magmatism [1-4]. Understanding the early earth evolution and its geodynamics is one of most fundamental scientific issues in geology, because the evolutionary trends of the planet earth cannot be resolved without adequate knowledge of Archean period. To understand the tectonic growth of continental crusts in Archean cratons, the granites are playing most important role in this context. The Bundelkhand Craton is nestled in the northern margins of Peninsular India. The Bundelkhand Craton begin with the ~3.5Ga crustal component growth signatures, as preserve in the form of TTG gneisses [5-7]. The Craton mainly constitutes older basement of TTG and mafic gneisses and is associated with migmatites, amphibolites, schist, and supra-crustal belt of meta-sedimentary and meta-volcanics. The ample potash-rich granites and granodiorite-granite series rocks mostly inhabit of the craton and crustal growth takes place during Neoproterozoic period in multiple phases [7-9]. Recently, Singh & Slabunov [10-13] depict the Greenstone Belts and establish tectonic evolution of the craton, based on SHRIMP-dating of zircon and geochemistry

from the felsic volcanic rocks from the Babina belt. The present paper deal with the geochemistry of granitoids (granodiorite-granite series and potash-rich granite) rocks from mostly central part of the Bundelkhand Craton to establish tectonic settings and the continental growth of the craton during Neoproterozoic period.

Geological Setting

The Bundelkhand Craton covers 29,000 km², lying between 24°11' to 26°27' N and 78°10' to 81°24' E, represents a semicircular outcrop. The low grade metamorphic rocks of the Bijawar Group (Paleoproterozoic) to the south, southeast, and Vindhyan Supergroup (Meso- to Neoproterozoic) to the southeast, south, southwest, and west are resting over on Bundelkhand Craton [7,14,15]. The major part of the craton comprises the different phases of magmatism, low-grade metamorphism and deformation of Archean TTG-gneissic rocks, mafic dykes and undeformed quartz veins [8,9,16-18]. The doleritic dykes are usually dark grayish green in color and have NNW-SSE to NW-SE trend [14,19]. A general characteristic of highly jointed quartz veins occur mostly about NE- SW to NNE-SSW trend. Slabunov & Singh [20] illustrate the greenstone belts from the central part of Bundelkhand Craton which are scattered in the E-W shear zones of 3-5kms width. The potash-rich granites

(~2.5 Ga) occurring around the Babina, Dhaura, and 3km south of the Mauranipur regions. The pegmatites veins are also observed at

many places. TTG-gneisses are exposed at the Babina, Dhaura, Gora and Mauranipur areas (Figure 1).

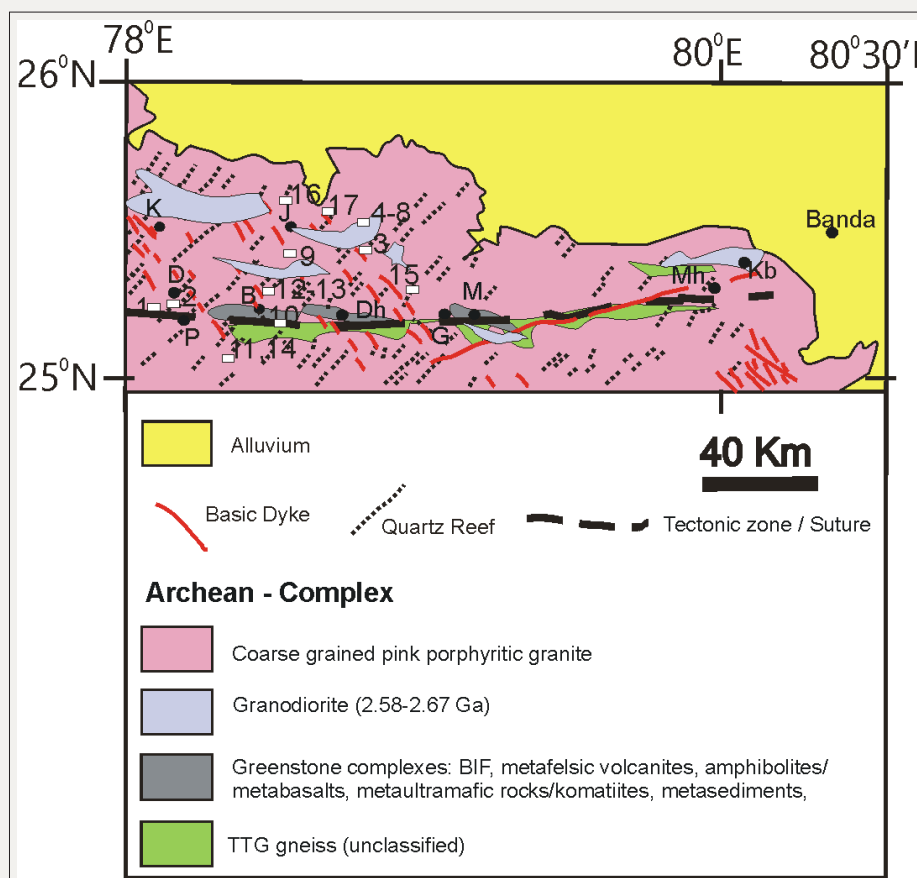


Figure 1: General geological map of central Bundelkhand Craton showing sample locations.

Abbreviations: B: Babina; D: Dhala; Dh: Dhaura; G: Gora; J: Jhansi; K: Karera; Kb: Kabrai; M: Mauranipur; Mh: Mahoba; P: Pichhore

Methodology

Fresh samples of granodiorite-granite series rocks and potash-rich granite, from central Bundelkhand Craton have been collected, and pulverized in agate ball mill for geochemical analysis. For major element analysis, 1.2g sample powder was weighed and mixed with 6g lithium borate flux (consisting of 35.3% tetraborate and 64.7% metaborate). Further, the fusion bead method was used to prepare the glass bead at 1000 °C for ≈8 min in Pt-Au crucible for only major elements analysis. For selected trace element analysis, 9g of sample powder was pressed into a pellet using 1.2g Wax binding agent. Both, glass bead and pressed pellet analysis were carried out at Institute of Geosciences, University of Campinas (UNICAMP), Brazil for seven samples. Major oxides concentrations were determined by X-ray Fluorescence Spectrometer (XRF), utilizing fusion beads whereas trace elements were obtained by inductively coupled plasma-mass spectrometry (ICP-MS) in press pellets. The loss of ignition (LOI) determined by TGA furnace. The base metals were analyzed using four acid digestions method by ICP- atomic emission spectroscopy (ICP-AES). Whereas total carbon and sulfur obtained by Leco combustion techniques. Five samples (SCB-1, SCB-2, SCB-3, SCB-4 and SCB-5) for whole rock geochemical analyses

were conducted at Australian Laboratory services Pty. Ltd., Malaga, Western Australia, Australia. Five potash-rich granite samples (BL-5, BL-6, BL-29, BL-30, SB-31) for whole rock geochemistry are analyzed at Petrozavodsk, Russia and detail methodology is given in Singh & Slabunov [12].

Geochemistry and Tectonic Settings

Geochemical compositions of Neoproterozoic granitoid samples from the Bundelkhand Craton are summarized in Table 1 and Table 2. In TAS (Total alkali vs Silica) diagram, the samples are classified volcanic equivalent [21] as dacite (SCB-04, BH-8, BM-6), trachyte (SCB-01, SCB-05), rhyolite (SCB-02, SCB-03, BH-11, UM-4, BJ-1; PL-1). The majority of potash-rich granite rocks are classified as rhyolite, whereas granodiorite-granite series rocks plotted in dacite and trachydacite field (Figure 2a). The granodiorite-granite series rocks are mostly high-K calc-alkaline and potash-rich granites are varies from high-K calc-alkaline to shoshonite series in nature (Figure 2b) [22]. In granodiorite-granite series rocks Na_2O varies from 3.29 to 3.83wt% and K_2O content varies from 2.44 to 4.04wt.%. The Al_2O_3 content varies from 12.61 to 15.79wt. % (av. Al_2O_3 : 14.79wt. %) and SiO_2 having range from 61.63 to 74.2wt.%. The titanium (TiO_2) content is low ranging from 0.25 to 1.32 wt.%.

Table 1: Major (wt.%) and trace (ppm) element analytical data of granodiorite (1-6) and granite (7-17) rocks from the central part of the Bundelkhand Craton.

Sample	1	2	3	4	5	6	7	8	9
	BM-6	UM-4	BH-8	SCB-1	SCB-4	SCB-5	SCB-2	SCB-3	BJ-1
SiO ₂	61.63	74.2	62.13	63.21	63.23	62.93	71.81	73.72	68.36
TiO ₂	0.535	0.252	0.554	0.55	0.56	1.32	0.37	0.16	0.294
Al ₂ O ₃	14.92	12.61	15.39	15.46	15.79	14.57	13.92	13.9	15.18
Fe ₂ O ₃	5.98	1.95	5.96	5.84	5.6	6.82	2.83	1.41	2.81
MnO	0.092	0.038	0.095	0.12	0.1	0.09	0.05	0.03	0.051
MgO	3.24	0.72	3.77	2.26	2.66	1.58	0.64	0.25	0.79
CaO	4.66	2.98	4.13	3.49	4.92	3.75	1.03	1.32	2.86
Na ₂ O	3.47	3.71	3.69	3.83	3.68	3.29	3.19	3.19	3.9
K ₂ O	2.87	2.55	3.03	3.65	2.44	4.04	5.4	5.42	3.86
P ₂ O ₅	0.153	0.07	0.158	0.16	0.16	0.66	0.09	0.04	0.079
LOI	1.63	0.86	0.99	1.42	0.92	0.82	0.89	0.42	0.97
Cr	86	11.4	83	100	90	40	10	10	13.6
Ni	21.6	6.8	21.3	18	21	22	4	7	6.4
Co	0	0	0	19	19	14	11	14	
Sc	11	4	12	12	13	8	4	1	5
V	93	29	96	106	115	87	29	8	30
Cu	15.1	42	25	1	39	25	3	6	2.5
Pb	28.1	18	33.8	22	22	32	32	55	27
Zn	80	23.7	90	80	76	104	34	35	46
Bi	0	0	0	0.12	0.23	0.11	0.05	0.21	
In				0.026	0.014	0.037	0.018	0.007	
Sn				3	3	5	3	2	
Mo				<1	2	4	1	1	
S				0.01	0.05	0.05	0.01	0.01	
Sb				0.06	0.16	0.05	<0.05	<0.05	
Te				0.01	0.01	0.02	0.01	0.01	
Rb	91	87	101	150.5	77.7	167	216	242	154
Cs				1.29	6.24	3.43	1.05	5.19	
Ba	624	510	662	895	704	1000	787	492	757
Sr	337	251	308	285	436	334	154	164.5	247
Tl				0.1	0.32	0.65	0.06	0.25	
Ga	15.7	14.9	18.8	19	20.4	24.2	19.3	17.1	20.7
Li				30	120	30	10	30	
Ta				1	2.4	2.5	2.3	1.3	
Nb	9.6	10.4	9.4	9.5	9.6	42.2	20.3	7.2	11.9
Hf				3.8	4.5	16.2	10	3.9	
Zr	149	162	151	139	170	703	378	116	165
Y	19.1	15.8	21	18.9	20.4	41.3	38.9	9.1	22.4
Th	13.7	26.8	16	13.15	13.6	35.3	47.6	31.2	23
U				4.84	4.4	5.47	12.95	9.92	
La	26	34	29	33.9	33.6	145	112	35.2	40
Ce	70	58	66	63.4	68.6	298	211	64.6	72
Pr	0	0	0	7.75	7.78	34.1	24.3	7.16	

Nd	32	25	25	27.2	27.5	115	78	22.9	32
Sm				4.96	5.17	18.5	11.9	3.68	
Eu				1.19	1.1	2.47	1.31	0.71	
Gd				4.02	4.08	12.4	8.56	2.35	0
Tb				0.65	0.65	1.7	1.37	0.32	0
Dy				3.47	3.65	8.65	7.23	1.53	0
Ho				0.67	0.74	1.51	1.39	0.29	0
Er				1.98	2.03	3.79	3.84	0.88	0
Tm				0.28	0.32	0.54	0.56	0.14	0
Yb				1.85	1.96	3.09	3.42	1.13	0
Lu				0.27	0.31	0.47	0.47	0.2	0
Sr/Y	17.644	15.8861	14.6667	15.0794	21.3725	8.08717	3.95887	18.0769	11.0268
K ₂ O/Na ₂ O	0.82709	0.68733	0.82114	0.953	0.66304	1.22796	1.69279	1.69906	0.98974
Na ₂ O+K ₂ O	6.34	6.26	6.72	7.48	6.12	7.33	8.59	8.61	7.76

Table 2:

Sample	10	11	12	13	14	15	16	17
	SB-31	BL-30	BL-6	BL-5	BL-29	BH-11	KR-12	PL-1
SiO ₂	72.7	74.02	75.28	71.84	74.86	72.35	64.62	70.45
TiO ₂	0.34	0.13	0.11	0.23	0.1	0.196	1.83	0.328
Al ₂ O ₃	12.35	13.4	12.24	13.47	13.03	14.16	10.18	15.29
Fe ₂ O ₃	0.97	0.6	0.79	1.14	0.53	2.4	13.33	4.76
FeO	1.36	0.86	0.79	1.22	0.65			
MnO	0.04	0.02	0.03	0.05	0.01	0.034	0.023	0.08
MgO	0.71	0.29	0.14	0.71	0.47	0.42	1.01	1.4
CaO	1.46	1.02	0.51	1.24	0.44	0.82	0.52	0.34
Na ₂ O	3.36	3.47	3.68	3.56	3.68	4.06	0.07	0.12
K ₂ O	5	5.33	5.26	5.11	5.26	4.42	4.97	3.45
P ₂ O ₅	0.08	0.03	0.02	0.08	0.05	0.043	0.307	0.126
LOI	1.48	0.69	0.67	1.07	0.68	0.98	2.34	3.57
Cr	9	6		9		7.7	11	22.9
Ni	2.2	2	0.5	3.2	0.7	3.7	10.8	18.6
Co	45	33	46	28	33			
Sc			3			3	22	3
V	21	5		21		15.3	188	49
Cu	4	4	1	11	7	2.9	12.3	4
Pb	33	54	24	35	49	23	26.2	14.5
Zn	47	22	50	50	16	30	38	132
Bi	0.18	0.14	0.38	0.29	0.17			
Cd	3.38	2.21	3.03	2.05	1.74			
In	0.02		0.08	0.03				
Sn	4.8	5.15	2.99	8	1.99			
Mo	2.64	2.94	2.55	0.38	1.12			
Sb	0.09	0.18	0.11	0.44	0.12			
Te		0.07	0.04					
Ag	0.1				0.1			
Rb	271	539	230	208	436	142	196	148

Cs	1.42	4.92	1.46	1.16	2.6			
Ba	596	222	78	975	215	1041	384	601
Sr	162	85	12	222	43	135	16.3	30
Tl	1.06	2.32	1.25	1.02	1.7			
Ga	17	25	22	25	23	18.3	11.9	18.2
Li	11.54	11.63	2.18	6.83	10.46			
Ta	2.38	7.84	2.03	2.24	4.73			
Nb	20.2	40.3	20.5	13.8	31.3	9.9	8.9	13.4
Hf	10.29	8.66	11.45	7.34	7.14			
Zr	306	193	293	193	147	218	188	163
Ti	2185	877	647	1604	571			
Y	35	56	35	24	34	15.7	67	26.8
Th	43.32	80.24	31.76	25.73	61.64	30.9	8.2	63
U	8.62	33.85	6.18	4.86	50.4			
La	110.59	82.59	88.27	58.19	24.89	63	<13	107
Ce	191.34	161.66	165.9	105.94	50.9	124	288	104
Pr	17.1	15.35	16.33	10.24	5.63			
Nd	62.91	54.55	61.11	37.34	21.92	43	82	36
Sm	10.49	9.9	10.4	6	4.81			
Eu	1.38	0.63	0.27	1.23	0.52			
Gd	9.64	9.63	9.71	5.68	5.01			
Tb	1.23	1.39	1.25	0.73	0.85			
Dy	6.61	8.31	6.73	3.99	5.4			
Ho	1.27	1.7	1.32	0.8	1.17			
Er	3.9	5.53	3.82	2.48	3.87			
Tm	0.56	0.9	0.54	0.37	0.64			
Yb	3.76	6.54	3.66	2.6	4.74			
Lu	0.54	0.97	0.52	0.39	0.75			
Be	4.39	7.92	3.02	2.74	5.92			
Sr/Y	4.62857	1.51786	0.34286	9.25	1.26471	8.59873	0.24328	1.1194
K ₂ O/Na ₂ O	1.4881	1.53602	1.42935	1.43539	1.42935	1.08867	71	28.75
Na ₂ O+K ₂ O	8.36	8.8	8.94	8.67	8.94	8.48	5.04	3.57

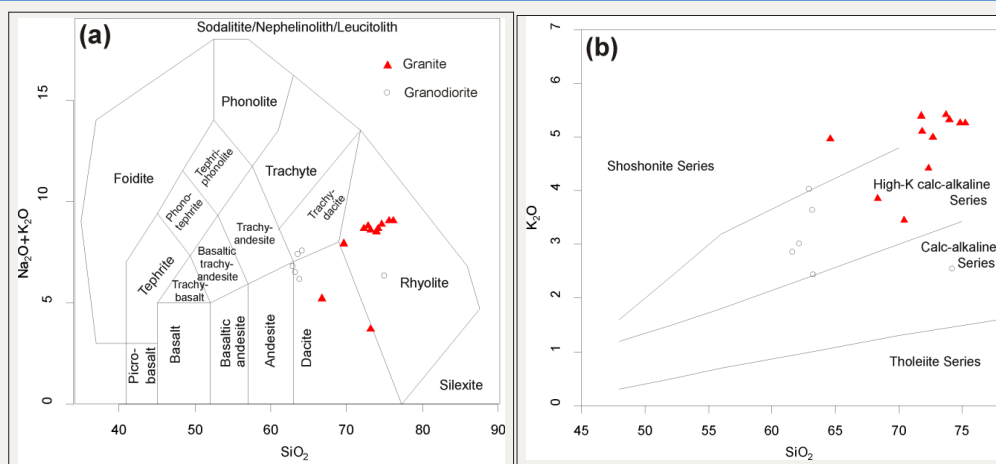


Figure 2: Classification diagram SiO₂ vs. Na₂O+K₂O [21].

Figure 2b: SiO₂ vs. K₂O diagram [22].

The potash-rich granite rocks having Na_2O varies from 3.19 to 4.06wt. % and K_2O content varies from 3.45 to 5.42wt. %. The Al_2O_3 content varies 10.18 to 15.18wt. % and SiO_2 having range from 64.62 to 75.28wt. %. The Titania (TiO_2) content are low ranging from 0.1 to 1.83wt. %. Most of the samples from granodiorite-granite series rocks are poor in potash ($\text{K}_2\text{O}/\text{Na}_2\text{O}$ varies from 0.66 to 1.22) while $\text{K}_2\text{O}/\text{Na}_2\text{O} > 1$ for potash-rich granite.

The granodiorite-granite series belongs to high-K calc alkaline magma series, with metaluminous character while potash-rich granite shows metaluminous to peraluminous character [23] (Figure 3). These granodiorite-granite series and potash-rich granite rocks mostly occur in I-type to A-type granitoids field of Whalen et al. [24]

diagram (Figure 4). On Harker diagram (Figure 5), the abundances of TiO_2 , Al_2O_3 , MgO , CaO , P_2O_5 , Fe_2O_3 and MnO decrease with linear or near-linear trends increasing SiO_2 on variation diagrams indicate a typical feature of I-type granites [25]. In the Yb+Ta versus Rb and Nb versus Y discrimination diagram of Pearce et al. [26], the granodiorite-granite series rocks plot within volcanic arc granite field whereas potash-rich granitic rocks plot within the syn-collision to post-collisional granite fields (Figure 6). This is also supported by the R1-R2 [$\text{R1}=4\text{Si}^{4+}-11(\text{Na}^++\text{K}^+)2(\text{Fe}^{3+}+\text{Ti}^{4+})$, molar; $\text{R2}=6\text{Ca}^{2+}+2\text{Mg}^{2+}+\text{Al}^{3+}$, molar] tectonic discrimination diagram (Figure 7) [27].

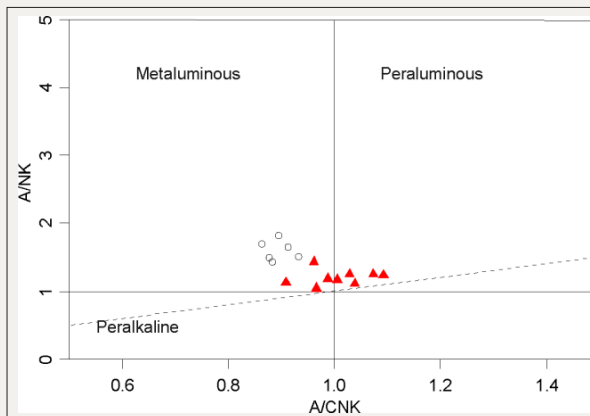


Figure 3: A/NK versus A/CNK diagram [23].

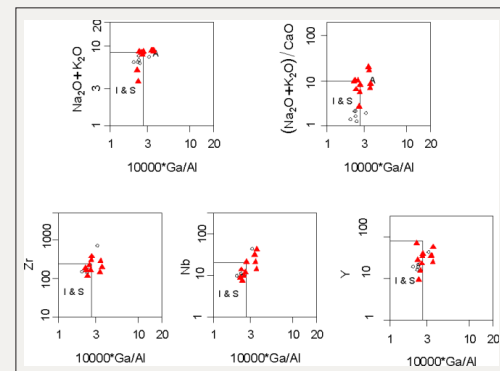


Figure 4: Classification of granitoids after Whalen et al. [24].

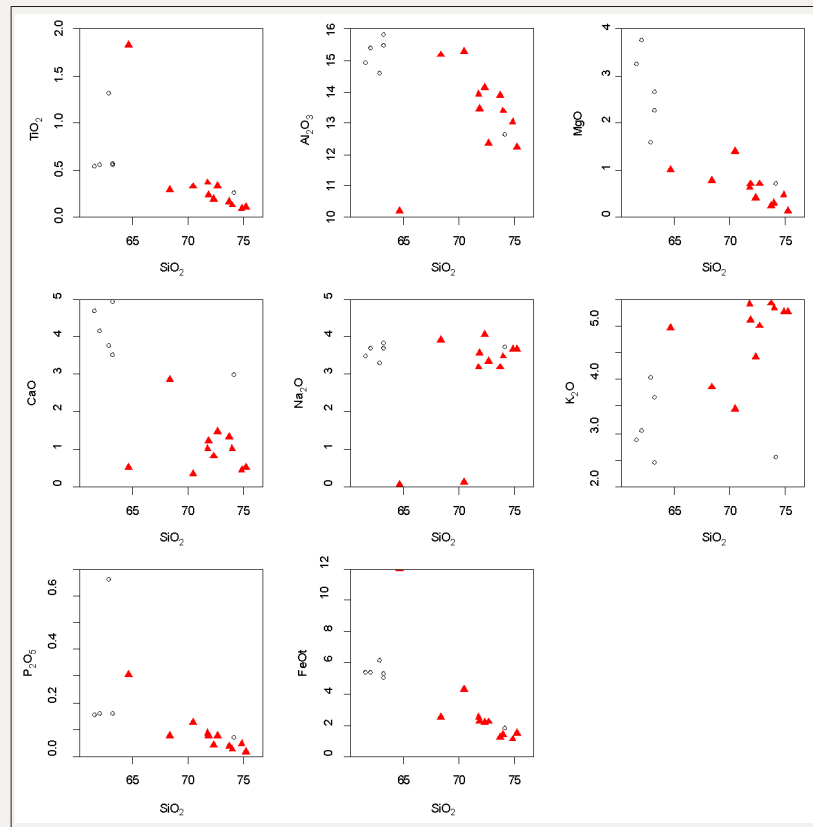


Figure 5: Harker diagrams for granitoid rocks from Bundelkhand Craton. Symbols are the same as in Figure 2.

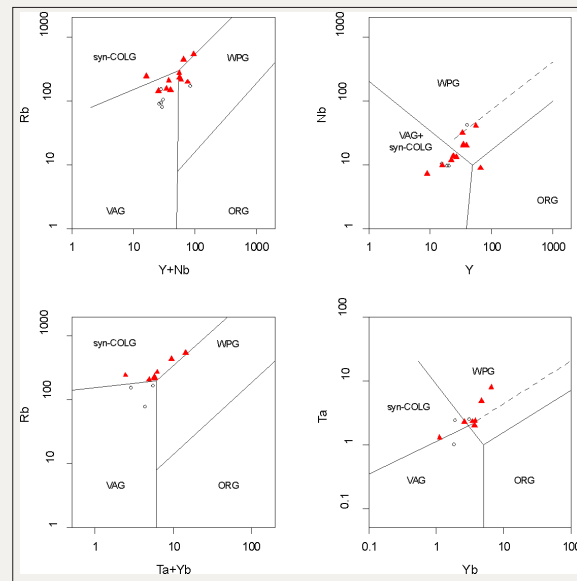


Figure 6: Discrimination diagrams Rb:Y+Nb, Nb:Y [26] for the TTG:gneiss and granite of the central Bundelkhand craton. Symbols are the same as in Figure 2.

ORG: Ocean Ridge Granites; syn: COLG: Syn: Collision Granites; VAG: Volcanic Arc Granites; WPG: Within Plate Granites

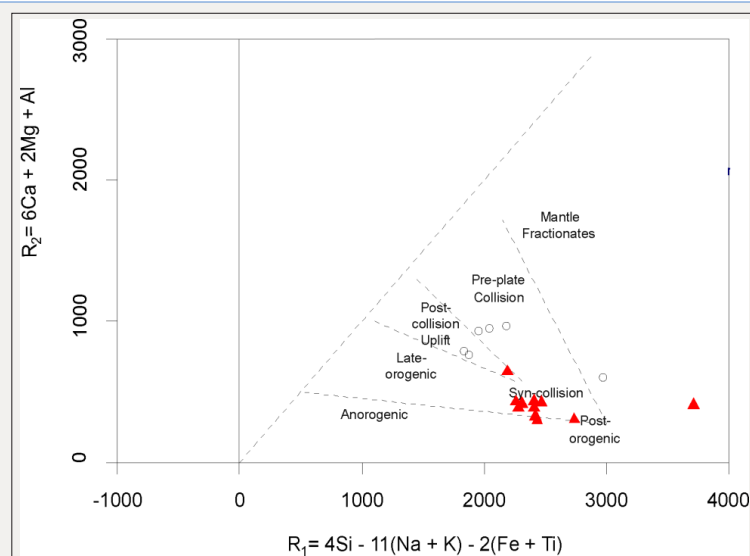


Figure 7: R1:R2 multicationic variation diagram [$R_1 = 4Si^{4+} - 11(Na^+ + K^+): (Fe^{3+} + Ti^{4+})$, molar; $R_2 = 6Ca^{2+} + 2Mg^{2+} + Al^{3+}$, molar], [27].

Discussion and Conclusion

The granodiorite-granite series samples are classified as dacite to rhyolite composition occur in subduction environment and potash-rich granites formed during syn-collision at shallow depth. The silica percentage ranging from 61–75wt% suggests acidic, calc-alkaline nature. It is characterized by relatively high Sr (12–436ppm), low Y (9.1–56) and low ratio of Sr/Y (0.34–21.37). Most of the potash-rich granite samples are rich in potash ($K_2O/Na_2O > 1$), with high Rb (77.7–539), moderate Nb (7.2–42.2) and Nd (21.92–115). The chondrite normalized rare earth element distribution pattern is poorly fractionated $La_N/Lu_N = (3.4–31.79)$ with a negative Europium (Eu) anomaly ($Eu/Eu^* = 0.2–0.82$) showing subduction environment (Figure 8a; [10,12,28]). A primitive mantle normalized [29] multi-element diagram (Figure 8b) showed a wide range in the concentration of the trace elements. Most of the samples show

enrichment of large-ion lithophile elements (LILE) but depletion of Nb, Ta and Ti [30]. The depletion of Nb and Ta in the rocks is most significant with Nb/La ratios (Figure 8b). It is noteworthy that the granodiorite-granite series and potash-rich granitic rocks are characterized by the Ba-poor, Sr, P, Nb-Ta and Ti anomalies. The negative Nb-Ta anomalies and a positive Pb anomaly are generally interpreted as subduction-related magma generation. Similarly, High-Field-Strength Elements (HFSE) depletions are common in rocks formed in arc environments, those that have interacted with continental crust, or those, which crystallized Ti-rich phases [31].

The Harker diagram of granitoids show positive correlation of K_2O vs. SiO_2 suggest that K-feldspar fractionation is an important differentiation process during the late stages of crystallization for the potash-rich granite in the Bundelkhand Craton [15]. Most of the samples are occur in I- to A-type granitic field of the Whalen

et al. [24] diagram which indicates that the granitoids are formed during syn-collision to post-collision tectonic environment. Singh & Singh [15] have established similar observation for the granites and TTG from central part of the Bundelkhand craton. The geochemical analysis suggests a subduction tectonic setting for granodiorite-granite series formed in active continental edge where oceanic crust subducted under continental block in Neoproterozoic time by

accretion-collision system. Chauhan et al. [16] also indicate that anhydrous partial melting of the Paleo-Mesoarchean TTG or mafic crustal materials in an extensional regime produce K-rich granites. The plagioclase-orthoclase granite advanced in post-accretionary processes after granodiorite-granite series formed in the craton. The Bundelkhand Craton stabilized at around 2.5Ga.

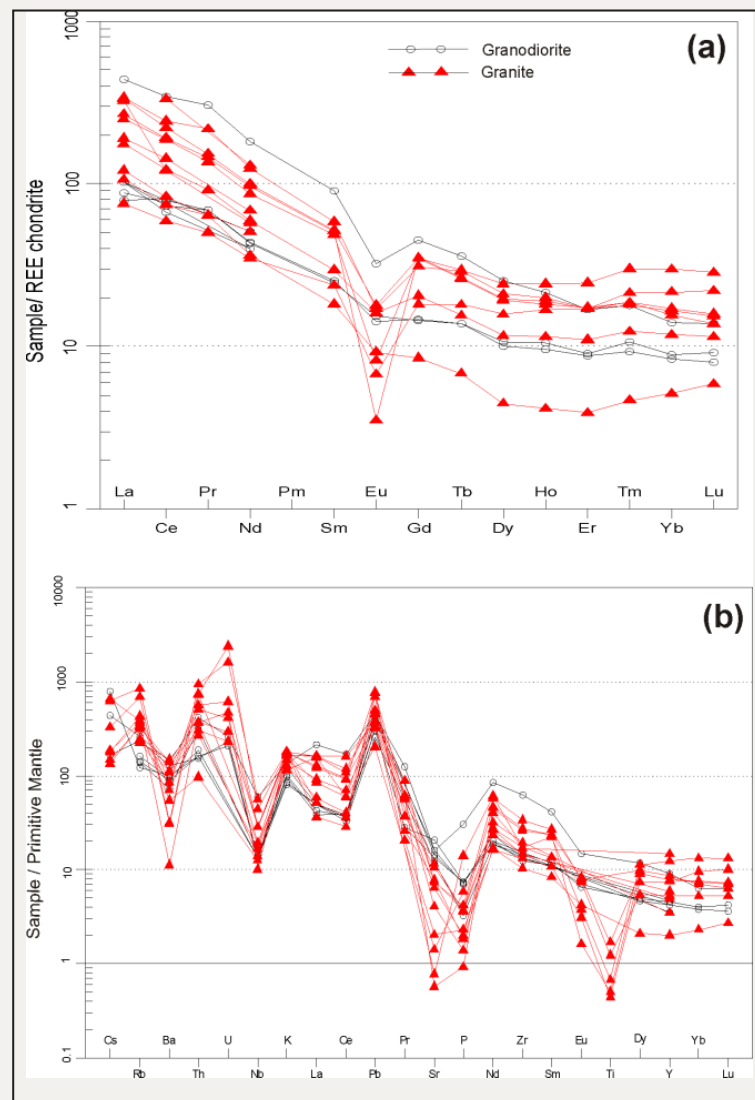


Figure 8: REE Chondrite spider plot after Nakamura [28].

Figure 8b: Primitive mantle-normalized elements [29] for the Neoproterozoic granitoids.

Acknowledgement

SM is thankful to DST Inspire fellowship [DST/INSPIRE/03/2015/000761] for providing financial support. PKS thankful to Association of Applied Geochemist (AAG) for partial analytical support at ALS laboratory, Western Australia for analysis of 5 samples. VKS expresses his cordial gratitude to the Department of Science and Technology, Gov. of India for [grant #INT/RUS/RFBP/P-279] and AIS is grateful to RFBP for [grant #17-55-45005 IND-a]. VKS gratefully acknowledge to Bundelkhand University,

Jhansi, India and IPICYT, Mexico, under MOU for supporting the research work. We are grateful to Sanjeet K Verma (IPICYT, Mexico) for his kind suggestions.

References

- Chandra R, Singh VK, Sivaji Ch, Piper JDA (2007) Precambrian continental growth and tectonism: Introduction. *Gondwana Research* 12(3): 199-201.
- Condie KC, Davaille A, Richard C, Aster RC, Arndt N (2015) Upstairs-downstairs: Supercontinents and large igneous provinces, are they

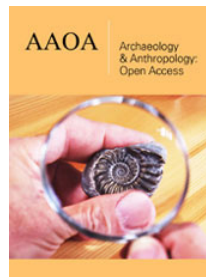
- related? *International Geology Review* 57: 1341-1348.
3. Singh VK, Chandra R, Basu AR, Verma SP, Biswal TK (2015) Precambrian crustal growth and tectonics: Introduction. *International Geology Review* 57(11-12): 5-8.
 4. Slabunov AI, Singh VK (2011) Archaean crustal evolution of the Fennoscandian and Bundelkhand craton: Prospective. In: Singh VK, Chandra R (Eds.), *Precambrian Continental Growth and Tectonism*, pp. 3-12.
 5. Kaur P, Zeh A, Chaudhri N, Eliyas N (2016) Unravelling the record of Archaean crustal evolution of the Bundelkhand Craton, northern India using U-b zircon-monzite ages, Lu-Hf isotope systematics, and whole-rock geochemistry of granitoids. *Precambrian Research* 281: 384-413.
 6. Saha L, Frei D, Gerdes A, Pati JK, Sarkar S, et al. (2016) Crustal geodynamics from the Archaean Bundelkhand Craton, India: constraints from zircon U-Pb-Hf isotope studies. *Geological Magazine* 153(1): 79-192.
 7. Sarkar A, Paul DK, Potts PJ (1996) Geochronology and geochemistry of the Mid-Archaean, Trondhjemitic gneisses from the Bundelkhand craton, Central India. *Recent Researches in Geology* 16: 76-92.
 8. Joshi KB, Bhattacharjee J, Rai G, Halla J, Ahmad T, et al. (2017) The diversification of granitoids and plate tectonic implications at the Archaean-Proterozoic boundary in the Bundelkhand craton, Central India. In: Halla J, Whitehouse MJ, Ahmad T, Bagai Z (Eds) *Crust-Mantle Interactions and Granitoid Diversification: Insights from Archaean Cratons*. Geological Society, London, Special Publications 449: 123-157.
 9. Verma SK, Verma SP, Oliveira EP, Singh VK, Moreno JA (2016) LA-SF-ICP-MS zircon U-Pb geochronology of granitic rocks from the central Bundelkhand greenstone complex, Bundelkhand craton, India. *Journal of Asian Earth Sciences* 118: 125-137.
 10. Singh VK, Slabunov A (2016) Two types of Archaean supracrustal belts in the Bundelkhand craton, India: Geology, geochemistry, age and implication for craton crustal evolution. *Journal of the Geol Soc of India* 88(5): 539-548.
 11. Singh VK, Slabunov A (2013) The greenstone belts of the Bundelkhand craton, Central India: New geochronological data and geodynamic setting. In: Singh VK, Chandra R (Eds.), *International Association for Gondwana research Conference Series No. 16, 3rd International conference Precambrian Continental Growth and Tectonism, Jhansi, India*, pp. 170-171.
 12. Singh VK, Slabunov A (2015a) The central Bundelkhand Archaean greenstone complex, Bundelkhand craton, central India: geology, composition, and geochronology of supracrustal rocks. *International Geology Review* 57(11-12): 1349-1364.
 13. Singh VK, Slabunov A (2015b) Geochemical characteristics of banded iron formation and metavolcanics of Babina greenstone belt of the Bundelkhand Craton, Central India. *J Econ Geol Georesource Management* 10: 63-74.
 14. Basu AK (1986) Geology of parts of Bundelkhand granite massif, Central India. *Record Geological Survey of India* 117: 61-124.
 15. Singh MM, Singh VK (2011) Geochemistry and tectonic setting of the TTG-gneiss and granite from central part of the Bundelkhand craton, India. In: Singh V K, Chandra R (Eds.), *Proceeding of the 2nd International Conference, Precambrian Continental Growth and Tectonism, USA*, pp. 95-102.
 16. Chauhan H, Saikia A, Ahmad T (2018) Episodic crustal growth in the Bundelkhand craton of central India Shield: Constraints from petrogenesis of the Tonalite-Trondhjemitic-Granodiorite gneisses and K-rich granites of Bundelkhand Tectonic Zone. *Journal of Earth System Science* 127: 44.
 17. Malviya VP, Arima M, Pati JK, Kaneko Y (2006) Petrology and geochemistry of metamorphosed basaltic pillow lava and basaltic komatiite in the Mauranipur area: subduction related volcanism in the Archean Bundelkhand craton, Central India. *Journal of Mineralogical and Petrological Sciences* 101(4): 199-217.
 18. Mondal MEA, Goswami JN, Deomurari MP, Sharma KK (2002) Ion microprobe $^{207}\text{Pb}/^{206}\text{Pb}$ ages of zircon from the Bundelkhand massif, northern India: Implication for crustal evolution of Bundelkhand-Aravalli protocontinent. *Precambrian Research* 117(1-2): 85-100.
 19. Sharma KK, Rahman A (2000) The Early Archaean-Palaeoproterozoic crustal growth of the Bundelkhand Craton, Northern Indian Shield. In: Dev M (Ed.), *Crustal Evolution and Metallogeny in the Northwestern Indian Shield*, pp. 51-72.
 20. Slabunov A, Singh VK (2018) Meso-Neoproterozoic crustal evolution of the Bundelkhand Craton, Indian Shield: new data from greenstone belts. *International Geology Review*: doi.10.1080/00206814.2018.1512906.
 21. Middlemost EAK (1994) Naming materials in the magma igneous system. *Earth-Science Review* 37(3-4): 215-224.
 22. Peccerillo A, Taylor SR (1976) Geochemistry of Eocene calc-alkaline volcanic rocks from the Kastamonu area, northern Turkey. *Contrib Mineral Petrol* 58(1): 63-81.
 23. Shand SJ (1943) Eruptive rocks: Their genesis, composition, classification, and their relation to ore-deposits with a chapter on meteorite, 2nd edition, New York, UK, pp. 1-444.
 24. Whalen JB, Currie KL, Chappell BW (1987) A-type granites: Geochemical characteristics, discrimination and petrogenesis. *Contributions to Mineralogy and Petrology* 95(4): 407-419.
 25. Chappel SW, White AJR (1974) Two contrasting granite types. *Pacific Geology* 8: 173-174.
 26. Pearce JA, Harris NBW, Tindle AG (1984) Trace element discrimination diagrams for the tectonic interpretation of granitic rocks. *Journal of Petrology* 25: 956-983.
 27. Batchelor RA, Bowden P (1985) Petro genetic interpretation of granitoids rock series using multicaticonic parameters. *Chem Geol* 48(1-4): 43-55.
 28. Nakamura N (1974) Determination of REE, Ba, Fe, Mg, Na and K in carbonaceous and ordinary chondrites. *Geochimica et Cosmochimica Acta* 38(5): 757-775.
 29. Sun SS, McDonough WF (1989) Chemical and isotopic systematics of oceanic basalts: Implications for mantle composition and processes. In: Saunders AD, Norry MJ (Eds.), *Magmatism in the Ocean Basins: Geological Society of London, Special Publications* 42: 313-345.
 30. McDonough WF, Sun SS (1995) The composition of the Earth. *Chemical Geology* 120: 223-253.
 31. Foley SF, Barth MG, Jenner GA (2000) Rutile/melt partition coefficients for trace elements and an assessment of the influence of rutile on the trace element characteristics of subduction zone magmas. *Geochimica et Cosmochimica Acta* 64(5): 933-938.



Creative Commons Attribution 4.0
International License

For possible submissions Click Here

[Submit Article](#)



Archaeology & Anthropology: Open Access

Benefits of Publishing with us

- High-level peer review and editorial services
- Freely accessible online immediately upon publication
- Authors retain the copyright to their work
- Licensing it under a Creative Commons license
- Visibility through different online platforms